Phase engineering of metal-organic frameworks

Ma, Chen; Zheng, Long; Wang, Gang; Guo, Jun; Li, Liuxiao; He, Qiyuan; Chen, Ye; Zhang, Hua

Published in:
Aggregate

Published: 01/02/2022

Published version (DOI):
10.1002/agt2.145

Publication details:
Ma, C., Zheng, L., Wang, G., Guo, J., Li, L., He, Q., Chen, Y., & Zhang, H. (2022). Phase engineering of metal-organic frameworks. *Aggregate*, *3*(1), Article e145. https://doi.org/10.1002/agt2.145

Received: 6 October 2021 | Revised: 31 October 2021 | Accepted: 10 November 2021

DOI: 10.1002/agt2.145

Aggregate WILEY

REVIEW

Phase engineering of metal-organic frameworks

Chen Ma[1] | Long Zheng[1] | Gang Wang[1] | Jun Guo[2] | Liuxiao Li[2] | Qiyuan He[3] | Ye Chen[1] | Hua Zhang[2,4,5]

[1] Department of Chemistry, The Chinese University of Hong Kong, Shatin, Hong Kong, China

[2] Department of Chemistry, City University of Hong Kong, Kowloon, Hong Kong, China

[3] Department of Materials Science and Engineering, City University of Hong Kong, Kowloon, Hong Kong, China

[4] Hong Kong Branch of National Precious Metals Material, Engineering Research Center (NPMM), City University of Hong Kong, Kowloon, Hong Kong, China

[5] Shenzhen Research Institute, City University of Hong Kong, Shenzhen, China

Correspondence
Ye Chen, Department of Chemistry, The Chinese University of Hong Kong, Shatin, Hong Kong, China.
Email: yechen@cuhk.edu.hk
Hua Zhang, Department of Chemistry, City University of Hong Kong, Kowloon, Hong Kong, China.
Email: Hua.Zhang@cityu.edu.hk

Funding information
The Chinese University of Hong Kong: Start-up, Grant/Award Number: 4930977; Direct Grant for Research, Grant/Award Number: 4053444; City University of Hong Kong, Grant/Award Numbers: 9610478, 9680314, 7020013, 1886921; Start-Up, Grant/Award Number: 9380100

Abstract

As an important category of porous crystalline materials, metal-organic frameworks (MOFs) have attracted extensive research interests owing to their unique structural features such as tunable pore structure and enormous surface area. Besides controlling the size, dimensionality, and composition of MOFs, further exploring the crystal-phase-dependent physicochemical properties is essential to improve their performances in various applications. Recently, great progress has been achieved in the phase engineering of nanomaterials (PEN), which provides an effective strategy to tune the functional properties of nanomaterials by modulating the arrangement of atoms. In this review, we adopt "phase" instead of "topology" to describe the crystal structure of MOFs and summarize the recent advances in phase engineering of MOFs. The two main strategies used to control the phase of MOFs, that is, phase-controlled synthesis and phase transformation of MOFs, will be highlighted. The roles of various reaction parameters in controlling the crystal phase of MOFs are discussed. Then, the phase dependence of MOFs in various applications including luminescence, adsorption, and catalysis are introduced. Finally, some personal perspectives about the challenges and opportunities in this emerging field are presented.

KEYWORDS

crystal phase, metal-organic frameworks, phase engineering, phase transformation, phase-controlled synthesis

1 | INTRODUCTION

Recently, phase engineering of nanomaterials (PEN)[1] has emerged as an important strategy to modulate the atomic arrangement of nanomaterials, which can further tune their physicochemical properties and functions.[2–6] Via PEN, a number of polymorphic nanomaterials, including metals[7–12] and transition metal dichalcogenides[13–15], and amorphous[16,17] and amorphous/crystalline heterophase nanomaterials[18–20] have exhibited outstanding performances in a wide range of promising applications. As a new kind of porous polymorphic materials, metal-organic frameworks (MOFs) have been extensively developed in the past decades.[21,22] Constructed by metal ions/nodes with organic linkers, MOFs possess large surface area, tunable chemical compositions, and long-range ordered pore structures, making them excellent candidates for versatile applications including gas storage,[23,24] separation,[25] catalysis,[26] drug delivery,[27] and optical device.[28,29] Importantly, in addition to size,[30,31] dimension,[32–36] and composition,[37] the phase of MOFs, that is, the ordered arrangement of building blocks, is also a key parameter to tune the performances of MOFs. To date, considerable progress has been made in the phase-controlled synthesis and phase transformation of MOFs.[38–40] It is of great importance to appreciate the achievement to date in phase engineering of MOFs and discuss the further extension of PEN strategies in MOFs.

In this review, we first give a brief introduction to the crystal phase of MOFs. Then, we highlight the phase engineering strategies in MOFs including direct phase-controlled synthesis and phase transformation. After that, phase-dependent

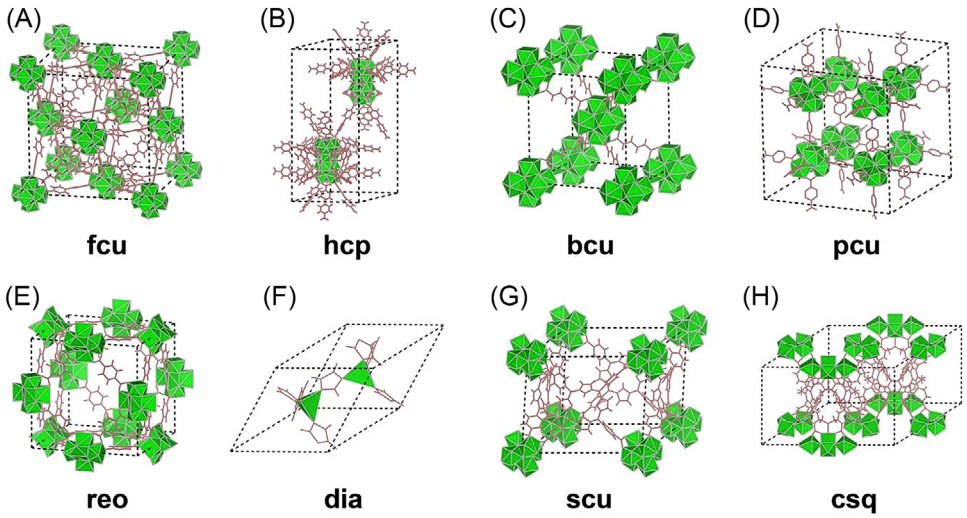

FIGURE 1 Schematic models of the unit cells of representative phases of MOFs. (A) face-centered cubic (**fcu**), (B) hexagonal close-packed (**hcp**), (C) body-centered cubic (**bcu**), (D) primitive cubic (**pcu**), (E) **reo** (named after ReO_3), (F) **dia** (named after diamond), (G) **scu** (built from square planar and cubical nodes), and (H) cube-and-square (**csq**). The green polyhedral, brown solid line and black dot line represent metal cluster, organic linker, and boundary of unit cells, respectively

performances of MOFs in applications including luminescence, adsorption, and catalysis are introduced. Finally, personal perspectives are provided to discuss the challenges and opportunities for this emerging field. This review opens the way for the rational design and preparation of novel MOFs and MOF-based materials in versatile applications via PEN strategies.

2 | CRYSTAL PHASE OF MOFS

Different terminologies can be used to describe the structures of MOFs. The more frequently used term, "topology," focuses on the connectivity of networks of MOFs[41,42] while *phase* emphasizes the packing mode of metal ions/nodes and linkers. To align with the terminology of PEN, in this review, we adopt "phase" to describe the ordered arrangements of metal nodes and linkers of MOFs. The unit cells of some representative phases of MOFs are shown in Figure 1. It is worth noticing that the abbreviations used in MOFs are sometimes different from those in other types of materials. For example, MOFs with face-centered cubic phase are denoted as "**fcu**" (Figure 1A), in which the metal nodes adopt a cubic close-packed fashion and are connected by 12 organic linkers. For metal nodes coordinated by 18 organic ligands, they often adopt a hexagonal close-packed (**hcp**, Figure 1B) fashion. Other commonly observed phases of MOFs including body-centered cubic (**bcu**, Figure 1C), primitive cubic (**pcu**, Figure 1D), reo (named after ReO_3, Figure 1E), **dia** (named after diamond, Figure 1F), **scu** (built from square planar and cubical nodes, Figure 1G), and cube-and-square (**csq**, Figure 1H) are also illustrated. In Table 1, detailed crystallographic information of MOFs discussed in this review are summarized, including linkers, metal clusters, phase, space group, and packing mode of metal clusters. Note that metal clusters with same packing mode can sometimes form different phases, which arises from different types of connectivity between metal clusters and linkers.

3 | PHASE ENGINEERING OF MOFS

3.1 | Direct phase-controlled synthesis of MOFs

In this section, direct synthesis strategies that can produce MOFs with different phases are introduced. The reported MOFs are categorized by the type of central metal, including Zr/Hf-MOFs, Mg-MOFs, Cu-MOFs, and In-MOFs.

3.1.1 | Zr/Hf-MOFs

The Zr/Hf-MOFs family is a representative example of polymorphic MOFs.[43,44] Based on the types of the organic linker, Zr/Hf-MOFs with polymorphs can be further classified to ditopic carboxylate ligand- and tetra-carboxylate ligand-based Zr/Hf-MOFs.

Ditopic carboxylate ligand-based Zr/Hf-MOFs

Zr-based UiO (University of Oslo) MOFs with the **fcu** structure were first reported by Cavka et al. in 2008.[45] By using the ditopic carboxylate ligands, including 1,4-benzenedicarboxylate (BDC), 4,4′-biphenyldicarboxylate (BPDC), and aminotriphenyldicarboxylate (TPDC), as the linker, UiO-66, UiO-67, and UiO-68 with **fcu** phase were obtained, respectively. While UiO MOFs normally crystallize into a **fcu** phase,[34] non-**fcu** phase UiO MOFs, such as **reo**[46], **hcp**,[38] and **hns**,[39] have been synthesized by adjusting the reaction conditions. It is worth noting that the modulator acids play key roles in the synthesis of MOFs with novel phase. For example, using formic acid as the modulator can greatly increase the concentration of missing-cluster defects in MOFs. These cluster vacancies were formed along < 100 > directions of the **fcu** matrix, leading to the formation of the **reo** UiO-66(Hf) (Figure 2A).[46] In the mid-2010s, Lin's group synthesized a series of Zr/Hf-based hexagonal UiO MOFs with non-**fcu** phase by using TPDC and quaterphenyldicarboxylate (QPDC) as linkers in the

TABLE 1 Summary of some representative reported MOFs with different phases

MOF	Phase	Linkers	Cluster	Space group	Packing mode of cluster*	Reference
UiO-66(Zr)	**fcu**	H_2BDC	$Zr_6(\mu_3\text{-}O)_4(\mu_3\text{-}OH)_4$	Fm-3 m	Cubic Close Packing	[45,85]
	hcp	H_2BDC	$Zr_{12}(\mu_3\text{-}O)_8(\mu_3\text{-}OH)_8(\mu_2\text{-}OH)_6$	P6(3)/mmc	Hexagonal Close Packing	[51,52,57,59]
UiO-66(Hf)	**fcu**	H_2BDC	$Hf_6(\mu_3\text{-}O)_4(\mu_3\text{-}OH)_4$	Fm-3 m	Cubic Close Packing	[39]
	fcu	H_2F_4BDC	$Hf_6(\mu_3\text{-}O)_4(\mu_3\text{-}OH)_4$	Fm-3 m	Cubic Close Packing	
	hcp	H_2BDC	$[Hf_6(\mu_3\text{-}O)_4(\mu_3\text{-}OH)_4]_2(\mu_2\text{-}OH)_6$	P6(3)/mmc	Hexagonal Close Packing	
	hcp	H_2F_4BDC	$[Hf_6(\mu_3\text{-}O)_4(\mu_3\text{-}OH)_4]_2(\mu_2\text{-}OH)_6$	P6(3)/mmc	Hexagonal Close Packing	
	hns	H_2F_4BDC	$[Hf_6(\mu_3\text{-}O)_4(\mu_3\text{-}OH)_4]_2(\mu_2\text{-}OH)_6$	P6/mmm	Primitive Hexagonal Packing	
UiO-67(Zr)	**fcu**	H_2BPDC	$Zr_6(\mu_3\text{-}O)_4(\mu_3\text{-}OH)_4$	Fm-3 m	Cubic Close Packing	[45]
	hcp	H_2BPDC	$Zr_{12}(\mu_3\text{-}O)_8(\mu_3\text{-}OH)_8(\mu_2\text{-}OH)_6$	P6(3)/mmc	Hexagonal Close Packing	[50]
UiO-67(Hf)	**fcu**	H_2BPDC	$Hf_6(\mu_3\text{-}O)_4(\mu_3\text{-}OH)_4$	Fm-3 m	Cubic Close Packing	[38]
	hcp	H_2BPDC	$Hf_{12}(\mu_3\text{-}O)_8(\mu_3\text{-}OH)_8(\mu_2\text{-}OH)_6$	P6(3)/mmc	Hexagonal Close Packing	
	hcp	H_2BPDC	$Hf_{12}(\mu_3\text{-}O)_8(\mu_3\text{-}OH)_8(\mu_2\text{-}OH)_6$	P6(3)/mmc	Hexagonal Close Packing	[50]
	hns	H_2BPDC	$[Hf_6(\mu_3\text{-}O)_4(\mu_3\text{-}OH)_4]_2(\mu_2\text{-}OH)_6$	P6/mmm	Primitive Hexagonal Packing	[38,39]
	hxl	H_2BPDC	$[Hf_6(\mu_3\text{-}O)_4(\mu_3\text{-}OH)_4]_2(\mu_2\text{-}OH)_6$	P6/mmm	Primitive Hexagonal Packing	[38]
Zr_{12}-BPYDC	**hcp**	H_2BPYDC	$Zr_{12}(\mu_3\text{-}O)_8(\mu_3\text{-}OH)_8(\mu_2\text{-}OH)_6$	P6(3)/mmc	Hexagonal Close Packing	[50]
Hf_{12}-BPYDC	**hcp**	H_2BPYDC	$Hf_{12}(\mu_3\text{-}O)_8(\mu_3\text{-}OH)_8(\mu_2\text{-}OH)_6$	P6(3)/mmc	Hexagonal Close Packing	
UiO-68(Zr)	**fcu**	H_2TPDC	$Zr_6(\mu_3\text{-}O)_4(\mu_3\text{-}OH)_4$	Fm-3 m	Cubic Close Packing	[45]
	hcp	H_2TPDC	$Zr_{12}(\mu_3\text{-}O)_8(\mu_3\text{-}OH)_8(\mu_2\text{-}OH)_6$	P6(3)/mmc	Hexagonal Close Packing	[56]
UiO (Zr)	**fcu**	H_2DCDPA	$Zr_6(\mu_3\text{-}O)_4(\mu_3\text{-}OH)_4$	Fm-3 m	Cubic Close Packing	[58]
	hcp	H_2DCDPA	$Zr_{12}(\mu_3\text{-}O)_8(\mu_3\text{-}OH)_8(\mu_2\text{-}OH)_6$	P6(3)/mmc	Hexagonal Close Packing	
MOL(Zr)	**hxl**	H_2DCDPA	$Zr_6(\mu_3\text{-}O)_4(\mu_3\text{-}OH)_4$	P6/mmm	Primitive Hexagonal Packing	
EHU-30	**hex**	H_2BDC	$Zr_6(\mu_3\text{-}O)_4(\mu_3\text{-}OH)_4$	$P6_3/mmc$	Primitive Hexagonal Packing	[53,85]
CAU-38(Ce/Zr)	**bcu**	H_2PZDC	$CeZr_5(\mu_3\text{-}O)_4(\mu_3\text{-}OH)_4$	Pnnm	Body-centered Orthorhombic Packing	[55]
DUT-67	**reo**	H_2TDC	$Zr_6(\mu_3\text{-}O)_6(\mu_3\text{-}OH)_2$	Fm-3 m	—	[54]
DUT-69	**bct**	H_2TDC	$Zr_6(\mu_3\text{-}O)_4(\mu_3\text{-}OH)_4$	$P2_12_12_1$	Primitive Orthorhombic Packing	
MOF-545	**csq**	H_4TCPP	$Zr_6(\mu_3\text{-}O)_8$	P6/mmm	Primitive Hexagonal Packing	[61]

(Continues)

TABLE 1 (Continued)

MOF	Phase	Linkers	Cluster	Space group	Packing mode of cluster*	Reference
MOF-525	**ftw**	H_4TCPP	$Zr_6(\mu_3\text{-}O)_4(\mu_3\text{-}OH)_4$	Pm-3 m	Primitive Cubic Packing	[61,88]
NU-902	**scu**	H_4TCPP	$Zr_6(\mu\text{-}O)_4(\mu\text{-}OH)_4$	P4/mmm	Primitive Tetragonal Packing	[62]
PCN-221	**ftw**	H_4TCPP	$Zr_8(\mu_4\text{-}O)_6$	Pm-3 m	Primitive Cubic Packing	[63]
PCN-222	**csq**	H_4TCPP	$Zr_6(\mu_3\text{-}OH)_8$	P6/mmm	Primitive Hexagonal Packing	[64]
PCN-223	**shp**	H_4TCPP	$Zr_6(\mu_3\text{-}O)_4(\mu_3\text{-}OH)_4$	P6/mmm	Primitive Hexagonal Packing	[65,88]
PCN-224	**she**	H_4TCPP	$Zr_6(\mu_3\text{-}O)_4(\mu_3\text{-}OH)_4$	Im-3 m	—	[66]
PCN-225	**sqc**	H_4TCPP	$Zr_6(\mu_3\text{-}O)_4(\mu_3\text{-}OH)_4$	I4(1)/amd	Body-centered Tetragonal Packing	[67]
NU-1000	**csq**	H_4TBAPy	$Zr_6(\mu_3\text{-}OH)_4(\mu_3\text{-}O)_4(OH)_4(OH_2)_4$	P6/mmm	Primitive Hexagonal Packing	[73,99]
NU-901	**scu**	H_4TBAPy	$Zr_6(\mu_3\text{-}OH)_4(\mu_3\text{-}O)_4(OH)_4(OH_2)_4$	P4/mmm	Primitive Tetragonal Packing	[74,99]
NU-906	**scu**	H_4TCPB-Br_2	$Zr_6(\mu\text{-}O)_4(\mu\text{-}OH)_4$	P4/mmm	Primitive Tetragonal Packing	[75,76]
NU-1008	**csq**	H_4TCPB-Br_2	$Zr_6(\mu\text{-}O)_4(\mu\text{-}OH)_4$	P6/mmm	Primitive Hexagonal Packing	
NU-500	—	H_4TCPB-Br_2	$Zr_6(\mu\text{-}O)_4(\mu\text{-}OH)_4$	C2/m	—	[76]
NU-600	**she**	H_4TCPB-Br_2	$Zr_6(\mu\text{-}O)_4(\mu\text{-}OH)_4$	Pm-3 m	Primitive Cubic Packing	
$[Mg_3(BTDC)_3(DMF)_4]$•DMF	**pcu**	H_2BTDC	$Mg_3(RCOO)_6$	P-1	Triclinic Packing	[79]
$[Mg_3(BTDC)_3(DMF)_4]$	**sxb**	H_2BTDC	$Mg_3(RCOO)_6$	C2/c	—	
NTU-51	**sql**	H_2fip	Cu-based	P4/nmm	Primitive Tetragonal Packing	[82]
NTU-52	**dia**	H_2fip	Cu-based	$I4_122$	Diamond Packing	
ZMOF	**rho**	4,5-ImDC	In-based	Im-3 m	Body-centered Cubic Packing	[83]
	sod	4,5-ImDC	In-based	Fd-3c	Face-centered Cubic Packing	
PCN-250	**soc**	H_4ABTC	$Fe_3\text{-}\mu_3\text{-oxo}$	P-43n	Primitive Cubic Packing	[40]
PCN-250′	**soc**	H_4ABTC	$Fe_3\text{-}\mu_3\text{-oxo}$	C2/c	Base-centered Monoclinic Packing	
PCN-250′′	**soc**	H_4ABTC	$Fe_3\text{-}\mu_3\text{-oxo}$	R-3c	Primitive Hexagonal Packing	
bio-MOF-100	**dia-c**	H_2BPDC	$Zn_8(AD)_4O_{16}$	Cc	Diamond Packing Packing	[93]
	lcs	H_2BPDC	$Zn_8(AD)_4O_{16}$	Ia-3d	—	

*The deformable property of the topology leads to the fact that one topology may have more than one type of packing mode for metal clusters.

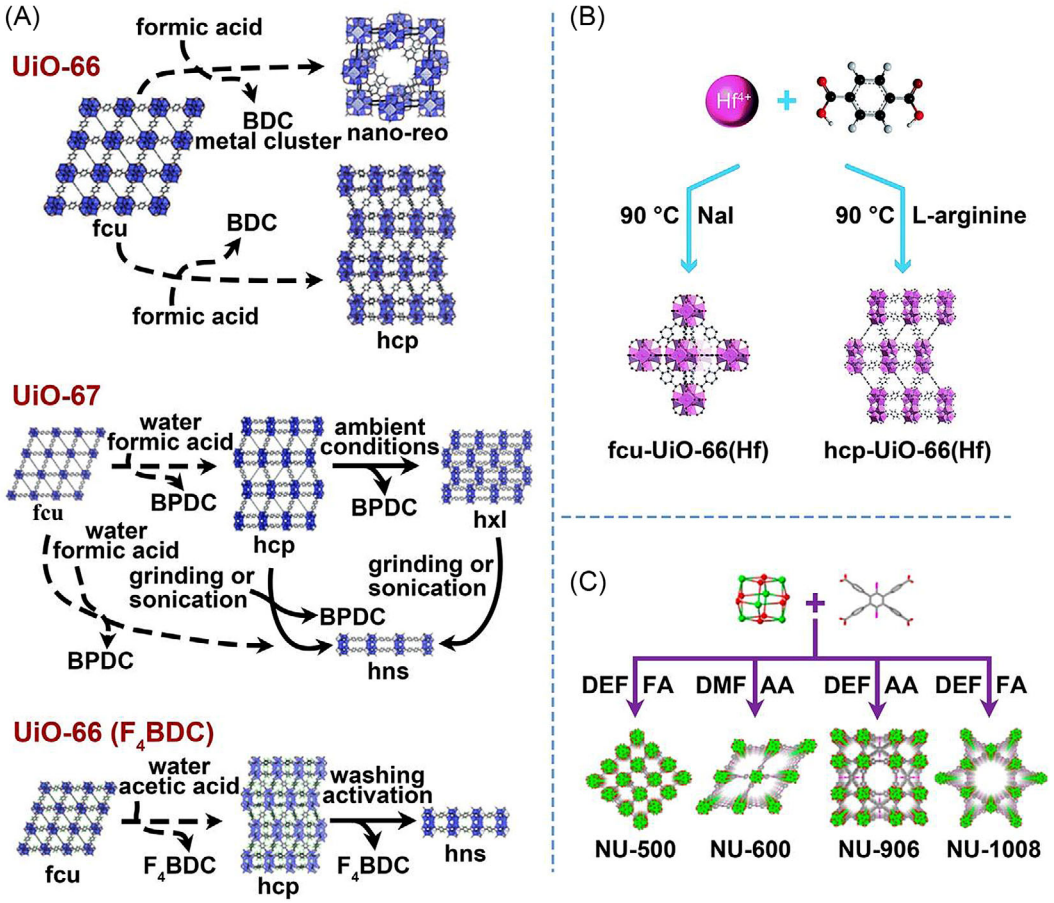

FIGURE 2 Direct synthesis of Zr/Hf-based MOFs with different phases. (A) The summary of the synthesis of UiO MOFs with varying phases. Dashed arrows and solid arrows show the differences in the synthesis conditions used to prepare different phases and post-synthetic treatments, respectively. Reproduced with permission: Copyright 2019, The Royal Society of Chemistry.[39] (B) The construction of Hf-based UiO-66 MOFs by adding salting-in ions. Reproduced with permission: Copyright 2019, The Royal Society of Chemistry.[59] (C) The synthesis of NU-500, NU-600, NU-906, and NU-1008 from H_4TCPB-Br_2 linker and Zr_6 node by adjusting solvents and modulators. DMF, DEF, FA and AA represent N,N-dimethylformamide, N,N-diethylformamide, formic acid, and acetic acid, respectively. Reproduced with permission: Copyright 2020, American Chemical Society[76]

presence of acetic acid as the modulator.[47–49] Their crystal phases were first recognized as the **fcu** phase with structural distortions,[47–49] and later proved to be **hcp** phase by Dai et al. in 2017.[50]

Prior to Dai et al., in the same year, Cliffe et al.[38] found that **hcp** UiO-67(Hf) could be synthesized at high temperature (≥ 130 °C) with a high concentration of formic acid as the modulator (Figure 2A). Compared with **fcu** UiO-67(Hf), the ligand:metal ratio in **hcp** UiO-67(Hf) increased from the 12:2 (typical ratio in **fcu** phase) to 18:2, resulting in the transformation from the 12-connected $Hf_6(\mu_3\text{-}O)_4(\mu_3\text{-}OH)_4$ metal node to the 18-connected $[Hf_6(\mu_3\text{-}O)_4(\mu_3\text{-}OH)_4]_2(\mu_2\text{-}OH)_6$ dimer via sharing six μ_2-OH bridges. The formation of the **hcp** phase UiO-67(Hf) may result from the low solubility of BPDC linker in the mixture of formic acid/N,N-dimethylformamide (DMF) and the condensation of the hafnium oxide nodes.[38] In 2018, Ermer et al. reported the synthesis of UiO-66(Zr) with **hcp** phase by using acetic acid as the modulator and ionic liquid di-(tributyl-ethoxymethyl-phosphonium)terephthalate ($[PBuMEE]_2[BDC]$) as both the solvent and the linker precursor.[51] By comparing different acid modulators including formic acid, acetic acid, and benzoic acid, they found that only acetic acid can lead to the formation of **hcp** UiO-66(Zr). Importantly, owing to the addition of $[PBuMEE]_2[BDC]$, almost all undesired impurities in obtained **hcp** UiO-66(Zr) could be removed easily by simply washing the product with water. In contrast, for **hcp** UiO-66(Zr) obtained with H_2BDC, Na_2BDC, or 1-ethyl-3-methylimidaziolium terephthalate ([EMIM][HBDC]) as linker, the unreacted linkers remain as impurity in the product due to their low solubility in water. As a result, the sample needs to be extracted by DMF and then washed by ethanol. In another work, UiO-66(Zr) with different phases were synthesized by adding hydrochloric acid (HCl) with different concentrations.[52] Specifically, at low HCl content (25 vol% and lower), UiO-66(Zr) with conventional **fcu** phase formed, whereas the increasing concentration of HCl to 50 vol% leads to the formation of **hcp** UiO-66(Zr). In addition, the EHU-30 (EHU: Euskal Herriko Unibertsitatea), reported as the first polymorph of UiO-66,[53] has been synthesized by using highly concentrated methacrylic acid as the modulator. The methacrylic acid can not only slow down the nucleation and crystal growth but also act as a template to direct the framework structure. As a result, each secondary building unit $[Zr_6(\mu_3\text{-}O)_4(\mu_3\text{-}OH)_4(\mu\text{-}COO)_{12}]$ is linked to eight surrounding clusters by 12 phenyl linkers, leading to the **hex** (primitive hexagonal lattice) phase instead of the **fcu** phase.

Other than UiO MOFs, other kinds of Zr- or Hf-based MOFs with different phases could also be synthesized by using acid modulators.[54,55] For instance, Bon et al. reported the phase-controlled synthesis of Zr-MOFs by using 2,5-thiophenedicarboxylic acid (H_2TDC)

as linkers and acetic acid as modulators.[54] When the amount of acetic acid (Ac) was ~120 molar equivalents of precursors, the 8-connected **reo** DUT-67(Zr) (DUT: Dresden University of Technology) (with a composition of $[Zr_6O_6(OH)_2(TDC)_4(CH_3COO)_2]$) and **reo** DUT-67(Hf) (with a composition of $[Hf_6O_6(OH)_2(TDC)_4(CH_3COO)_2]$) adopting primitive cubic packing were synthesized. Meanwhile, if the amount of acetic acid declined to 50 molar equivalents of precursors, the 10-connected body-centered tetragonal (**bct**) packing DUT-69(Zr) (with a composition of $[Zr_6O_4(OH)_4(TDC)_5(Ac)_2]$) and **bct** DUT-69(Hf) (with a composition of $[Hf_6O_4(OH)_4(TDC)_5(Ac)_2]$) were obtained. In another work, systematic investigations of the chemical system Ce^{4+}/Zr^{4+}/1-H-Pyrazole-3,5-dicarboxylic acid (H_2PZDC)/formic acid suggested that not only formic acid/metal ratio but also the ratio of metal precursor of Ce^{4+}/Zr^{4+} are important factors for the formation of MOFs with different phases.[55] Specifically, at molar ratios of formic acid/metal of 75:2 and Ce/Zr ratio < 0.8:1.2, the **fcu** UiO-66(Ce/Zr) (PZDC) structure was formed. The increasing Ce^{4+}/Zr^{4+} ratio leads to the formation of the mixture of **fcu** UiO-66(Ce/Zr) (PZDC) and **reo** DUT-67(Ce/Zr) (PZDC). At Ce/Zr ratio > 1.8:0.2, pure **reo** DUT-67(Ce) (PZDC) was formed. In another separate experiment, when the formic acid/metal ratio was fixed to 175:2 and the Ce^{4+}/Zr^{4+} ratio was varied (from 0:2 to 1.8:0.2), the as-obtained **reo** DUT-67(Ce/Zr) (PZDC) with tunable Ce/Zr ratios can be obtained. Further increasing the molar ratio of formic acid/metal to 350:2 at Ce^{4+}/Zr^{4+} ratios between 0.4:1.6 and 1.4:0.6 led to the formation of CAU-38(Ce/Zr) PZDC with **bcu** phase.

Besides using acid as a modulator to tune the phase of MOFs, the addition of water in the reaction mixture may also promote the formation of MOFs with novel phase. For instance, Ji et al. found that **hcp** UiO-68(Zr) can be obtained by adding a suitable concentration of water to the reaction mixture.[56] Recently, Firth et al. systematically demonstrated that the amount of water and acid in the reaction mixture play equally crucial roles in synthesizing UiO family MOFs with different phases (Figure 2A).[39] They first investigated the effect of formic acid on the phases of UiO-67(Hf) in the absence of water. When 20 vol% formic acid was added to the reaction mixture, **hcp** UiO-67(Hf) was formed. With increasing concentration of formic acid (> 20 vol %), UiO-67(Hf) with a phase resembling **hxl** (hexagonal lattice) was generated. Then, they investigated the effect of water concentration in the reaction mixture with a fixed volume of formic acid on UiO-67 phases. The result showed that adjusting the concentration of water in the synthesis could not only tune the phase of MOFs but also improve the phase purity. Specifically, pure **hcp** UiO-67(Hf) could be obtained by adding water, formic acid, and DMF in the volume ratio of 0.05:1:4. When the volume of water was changed from 0.05 mL to 0.2 mL, pure **hns** (hexagonal nanosheet) instead of **hcp** UiO-67(Hf) can be formed. Then, they found the phase of UiO-66(Hf) (F_4BDC) also depended on the ratio of water/modulator acid. With increasing ratio of water/acetic acid, **hcp** phase UiO-66(Hf) (F_4BDC) was formed first and then the UiO-66(Hf) (F_4BDC) with a phase similar to **hxl** was observed. Therefore, they proposed that simultaneously increasing the amount of water and acid may promote the formation of **hcp** phase. This was further demonstrated in the phase-controlled synthesis of UiO-66(Hf). Pure **hcp** UiO-66(Hf) could be synthesized under high concentrations of water and formic acid, whereas decreasing the concentration of either water or acid would promote the generation of **fcu** phase UiO-66(Hf). Chen et al. also indicated that both water and modulator acid were essential components for controlling the phase of UiO family MOFs.[57] In their work, UiO-66(Zr) with **hcp** phase was only obtained when the ratio of water/acetic acid was 1:1. Only a noncrystalline product or a zirconium acetate was formed when the amount of water or acetic acid was increased, respectively. Recently, Hu et al. found that not only the phase but also the morphology of UiO MOFs could be tuned by the addition of water or/and modulator acid.[58] **fcu** UiO(Zr) MOF with octahedral morphology was synthesized by using 4,4′-(9,10-anthracenediyl)dibenzoic acid (H_2DCDPA) as the linker and $ZrCl_4$ as the metal precursor in a mixture of DMF and acetic acid. If acetic acid was changed to trifluoroacetic acid, the shape of **fcu** UiO(Zr) became hexagonal nanoplate. In addition, changing the solution to a mixture of water and trifluoroacetic acid could produce **hxl** MOL (metal-organic layers). In another separate experiment, when water was added to the reaction mixture with a volume ratio of acetic acid/water of 2:1, the **hcp** phase UiO(Zr) with hexagonal nanoplate morphology instead of octahedral **fcu** UiO(Zr) could be obtained. These reports suggest that the addition of modulator acid or water and the regulation of their relative concentrations could be promising strategies to directly synthesize MOFs with different phases.

Different from adding water or modulator acid into reaction mixture, Li et al. introduced a self-assembly strategy induced by salting-in species to synthesize Zr- or Hf-based UiO-66 with **hcp** or **fcu** phase in an aqueous solution.[59] According to the Hofmeister effect,[60] the solubility of ligands (H_2BDC for UiO-66) in aqueous media could be enhanced with the use of salting-in ions. The **hcp** UiO-66(Zr) could be obtained by using salting-in ions with very limited solubilization capacity, like NO_3^-, I^-, ClO_4^-, SCN^-, and guanidinium (Gdm^+). When L-arginine, an extended and stronger salting-in ion, was used, the solubility of ligand (BDC) in aqueous solution was greatly increased, and the formation of the **fcu** phase instead of ligand-deficient **hcp** phase was observed. Similar to the synthesis of UiO-66(Zr), UiO-66(Hf) with **hcp** and **fcu** phase could also be synthesized using NaI and L-arginine as the mediator, respectively (Figure 2B).

Tetra-carboxylate ligand-based Zr/Hf-MOFs

Due to the abundant coordination sites in tetra-carboxylate ligands and the variable connectivity and symmetry of the Zr-based clusters, the combination of tetratopic carboxylic linkers and Zr-based inorganic units gives rise to multiple kinds of Zr-MOFs. 2,3,5,6-tetrakis(4-carboxyphenyl) pyrazine (TCPP) is one of the most popular tetracarboxylic linkers for constructing Zr-MOFs with different phases (Figure 3). At present, at least eight Zr-MOFs with different phases synthesized using H_4TCPP organic ligand have been reported. Specifically, Yaghi's group reported MOF-545 and MOF-525,[61] Farha's group prepared NU-902 (NU: Northwest University),[62] and Zhou's group synthesized a series of MOFs from PCN-221 to PCN-225 (PCN: porous coordination network).[63–67] By varying experimental conditions such as reaction temperature, types of modulators and

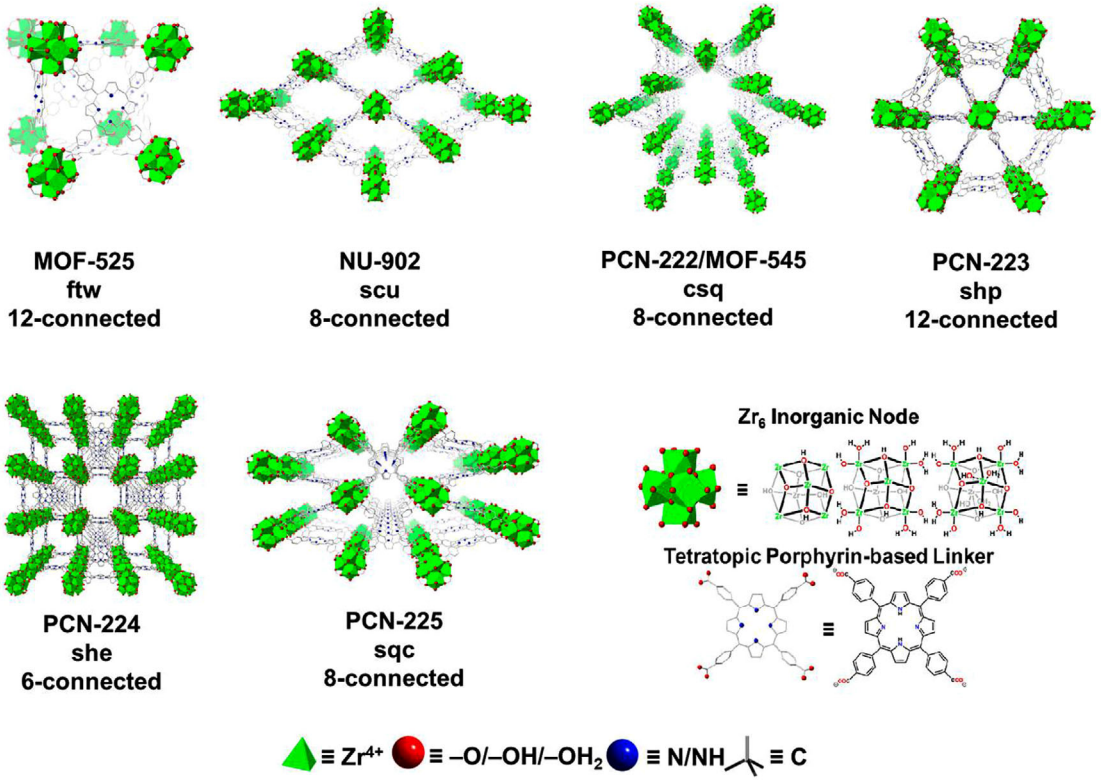

FIGURE 3 Direct synthesis of Zr-MOFs with different phases built from Zr_6 clusters and $TPPC^{4-}$ ligand. Reproduced with permission: Copyright 2019, American Chemical Society[70]

starting precursors (i.e. metal salts), and their concentrations and mutual ratios, various porphyrinic Zr-MOFs with different packing phases could be obtained. The first example of TCPP-based Zr-MOFs was reported by Morris et al. in 2012.[61] In this work, the authors synthesized two kinds of Zr-MOF crystals with different phases, namely MOF-545 and MOF-525. They used zirconyl chloride octahydrate as the metal precursor and formic acid as the modulator to prepare MOF-545 crystal in a DMF solution. The MOF-545 is constructed by $Zr_6(\mu_3\text{-O})_8$ node and each node connects with eight ligands, which features a (4,8)-connected csq phase. In addition, there were triangular-shaped and hexagonal-shaped one-dimensional (1D) channels in the structure of MOF-545, with cavity diameters of 8 Å and 36 Å, respectively. By increasing the reaction temperature, decreasing the ratio of Zr precursor/H_4TCPP, and adding acetic acid as modulator rather than formic acid, MOF-525 with a (4,12)-connected **ftw**[61] structure was prepared. Different from the 1D channel structures observed in MOF-545, in MOF-525, cubic cage composed of eight corner-sharing $Zr_6(\mu_3\text{-O})_4(\mu_3\text{-OH})_4$ clusters and six face-sharing porphyrin units with an edge length of 20 Å was observed. Using the same substrate identities as this work, NU-902 was obtained by Deria et al. at a lower synthesis temperature using benzoic acid as a modulator.[62] The structure of NU-902 is built by 8-connected $Zr_6(\mu_3\text{-O})_8$ nodes and features a new (4,8)-connected **scu** structure.

Parallel to the work of Morris et al., PCN-222 with the same structure as MOF-545 was reported by Feng et al.[64] at nearly the same time. Different from the reaction condition of MOF-545, $ZrCl_4$ was used as the metal precursor with benzoic acid as modulator to synthesize PCN-222 in a N,N-diethylformamide (DEF) solution. Following this work, PCN-225 with the rarely reported (4,8)-connected **sqc**[68] phase was obtained by using both benzoic acid and acetic acid as modulators.[67] The structure of PCN-225 possesses two types of pores: the small quadrangle-shaped cavity with a size of 15 Å and the big pear-like one of 22 Å. By choosing acetic acid as the only modulator, a novel Zr-MOF was explored, denoted as PCN-221.[63] Like MOF-525, PCN-221 also crystallizes via the primitive cubic packing in the **ftw** phase. However, in PCN-221, each $TCPP^{4-}$ organic ligand is combined with four novel Zr_8 cubic units instead of the classical Zr_6 octahedron. In addition, the structure of PCN-221 features cubic and distorted octahedral cavities with diameters of 20 Å and 11 Å, respectively. When the solvent is changed from DEF to DMF, PCN-223 and PCN-224 could be obtained by applying acetic acid and benzoic acid as the modulators, respectively.[65,66] The phase of PCN-223 is hexagonal packing with another (4,12)-connected **shp**[69] structure. In PCN-223, each $Zr_6(\mu_3\text{-O})_4(\mu_3\text{-OH})_4$ unit connects with twelve porphyrinic linkers, which forms uniform triangular 1D cavities of 12 Å along the c axis. As for PCN-224, there are three-dimensional (3D) channels with a diameter of 19 Å in its (4,6)-connected **she**[69] structure. Importantly, the ratio of $ZrCl_4$/H_4TCPP was varied while the reaction temperature (120°C) was kept constant in synthesizing PCN-222 series.

Recently, some reports aimed to understand the correlation between experimental parameters and the structure of Zr-TCPP MOFs by controlling reaction variables. For example, Gong et al. analyzed the effect of reaction temperature on the phase structure of porphyrinic Zr-MOFs while keeping other variables constant (Figure 3).[70] The synthesis at room temperature resulted in products with a mixed phase consisting of MOF-525 and PCN-224 with **ftw** and **she** structures, respectively, while a mixture of **csq** PCN-222, **shp** PCN-223, and **scu** NU-902 was obtained when the temperature was raised

to 145°C. At the same temperature, the **csq** PCN-222 would dominate in the product when the reaction time was further increased to 7 days, indicating that MOF-525 and PCN-224 were the kinetically preferred products while PCN-222 was the thermodynamically preferred product. In another example, Shaikh et al. investigated the effect of the modulator on the synthesis of Zr-TCPP MOFs.[71] Using strong acids such as difluoroacetic acid, formic acid, and nitrobenzoic acid as a modulator facilitated the formation of PCN-222. PCN-223 tended to form by employing less acidic modulators, like glacial acetic acid, propionic acid, and 4-chlorobenzoic acid, while employing weak acids such as 4-methoxybenzoic acid, decanoic acid, myristic acid, and stearic acid as a modulator led to the formation of MOF-525. The function of modulators could arise from the induction of different kinds of defect sites in Zr-based MOFs.[72] The authors proposed that strong acidic modulators (difluoroacetic acid and formic acid) and sterically demanding modulators (myristic acid and stearic acid) would produce missing cluster defects, while the less acidic modulators (propionic acid) mainly generated missing linker defects. Therefore, the modulator acidity could be the key in determining the defect structures and thus phases of MOFs.

Besides TCPP, 1,3,6,8-tetrakis(*p*-benzoate)pyrene (TBAPy) and 1,4-dibromo-2,3,5,6-tetrakis(4-carboxyphenyl)benzene (TCPB-Br_2) are the other two kinds of tetratopic carboxylate ligands used in phase-controlled synthesis of Zr-MOFs. In the case of $TBAPy^{4-}$ ligand, NU-901 and NU-1000, two Zr-MOFs with identical building blocks but different phases, have been successfully reported. **csq** NU-1000 was prepared by Mondloch et al. by using $ZrCl_4$ as the metal precursor and benzoic acid as a modulator.[73] The **csq** NU-1000 possesses mesoporous 31 Å hexagonal-shaped cavities and microporous 12 Å triangular-shaped cavities. When the modulator was changed to 4-amino-benzoic acidic, NU-901 with pure **scu** phase was obtained.[74] The **scu** NU-901 features a diamond channel of 29 Å in length and 12 Å in width. The TCPB-Br_2 is another representative flexible linker and its conformation could be tuned to synthesize Zr-MOFs with different phases. For example, Lyu et al. reported that **scu**-NU-906 and **csq**-NU-1008 could be built from the Zr_6 nodes and H_4TCPB-Br_2 linker when benzoic acid and formic acid were used as modulators in DMF, respectively.[75] Then, Chen et al. reported the preparation of **scu**-NU-906 and **csq**-NU-1008 by using different modulators or solvents.[76] As shown in Figure 2C, when the solvent and modulator were changed to DEF and formic acid, respectively, the NU-1008 was synthesized. However, when choosing DMF as the solvent and acetic acid as the modulator, the NU-906 was obtained. Furthermore, the evolution from 8-connected Zr_6 nodes to 6-connected Zr_6 nodes would be observed when DMF was replaced with DEF, resulting in the formation of **she**-NU-600. Note that in this experiment changing merely the solvent could result in the phase-controlled synthesis of MOFs. The authors proposed that the stronger basicity of DEF than DMF would increase the deprotonation rate of TCPB-Br_2^{4-} linker, leading to a fast nucleation and slow growth process to form the lower 6-connected Zr_6 nodes. Interestingly, after the modulator was altered from acetic acid to formic acid, the NU-500 with 5-connected Zr_6 nodes was formed. The stronger competition of formate with TCPB-Br_2^{4-} linker led to a lower coordination of NU-500 node.

Compared to the many reports about the phase-controlled synthesis of Zr/Hf-MOFs, reports of other kinds of MOFs with different phases are relatively limited. This may be explained by the high oxidation state of Zr/Hf(IV) in Zr/Hf-MOFs compared with M(I), M(II), and M(III) in M-MOFs (M stands for metal) and tunable connection number of Zr_6/Hf_6 cluster without altering the robust [Zr_6/Hf_6(μ_3-O)$_4$(μ_3-OH)$_4$] core.[77] In the following parts, Mg-MOFs, Cu-MOFs, and In-MOFs with different phases prepared by direct synthesis methods are briefly discussed.

3.1.2 | Mg-MOFs

In Mg-MOFs, the trinuclear carboxylate unit $Mg_3(RCOO)_6$ is a common 6-connected node, which is often organized in a 3D network with the **pcu** phase.[78] It has been reported that the $Mg_3(RCOO)_6$ building units can be linked by the linear 2,2′-bithiophen-5,5′-dicarboxylate (H_2BTDC) ligand to synthesize two 3D MOFs with different structures via a temperature-controlled crystallization process.[79] As a result, the [Mg_3(BTDC)$_3$(DMF)$_4$]·DMF with a common **pcu** (low-temperature phase) and [Mg_3(BTDC)$_3$(DMF)$_4$] with a rare **sxb** (six-coordinated net, b type[80,81]) (high-temperature phase) have been prepared by tuning the orientation of $btdc^{2-}$ anions under different reaction temperatures. Specifically, the [Mg_3(BTDC)$_3$(DMF)$_4$]·DMF and [Mg_3(BTDC)$_3$(DMF)$_4$] feature the parallel and semi-parallel arrangement of the $btdc^{2-}$ linkers, respectively.

3.1.3 | Cu-MOFs

As for Cu-MOFs, Liu et al. reported that the reaction of copper nitrate and 5-(furan-2-yl)isophthalic acid (H_2fip) in a DMF/H_2O solution led to the formation of NTU-51 (NTU: Nanjing Tech University) with 2D planar **sql** (square lattice) phase of the Cu-paddlewheel clusters by adding a trace amount of HNO_3, while the 3D diamond-like **dia** NTU-52 was obtained in absence of HNO_3.[82] The carboxylate groups of the fip ligands around the Cu-paddlewheel clusters possessing different coordination orientations and different rotations of carboxylate groups caused the distinct structural difference.

3.1.4 | In-MOFs

The phase tuning of the In-based zeolite-like MOFs (ZMOFs) was investigated by Shi et al. via tuning the concentration of structure-directing agents.[83] The morphology and phase evolution from porous **rho** (rho topology[84]) ZMOF particles to non-porous sphere-like **sod** (sodalite topology[84])-ZMOF has been achieved by gradually increasing the concentration of hexamethylenetetramine, which performed as both structure-directing agent and space-filling species to fill the cages and channels and therefore form a non-porous structure.

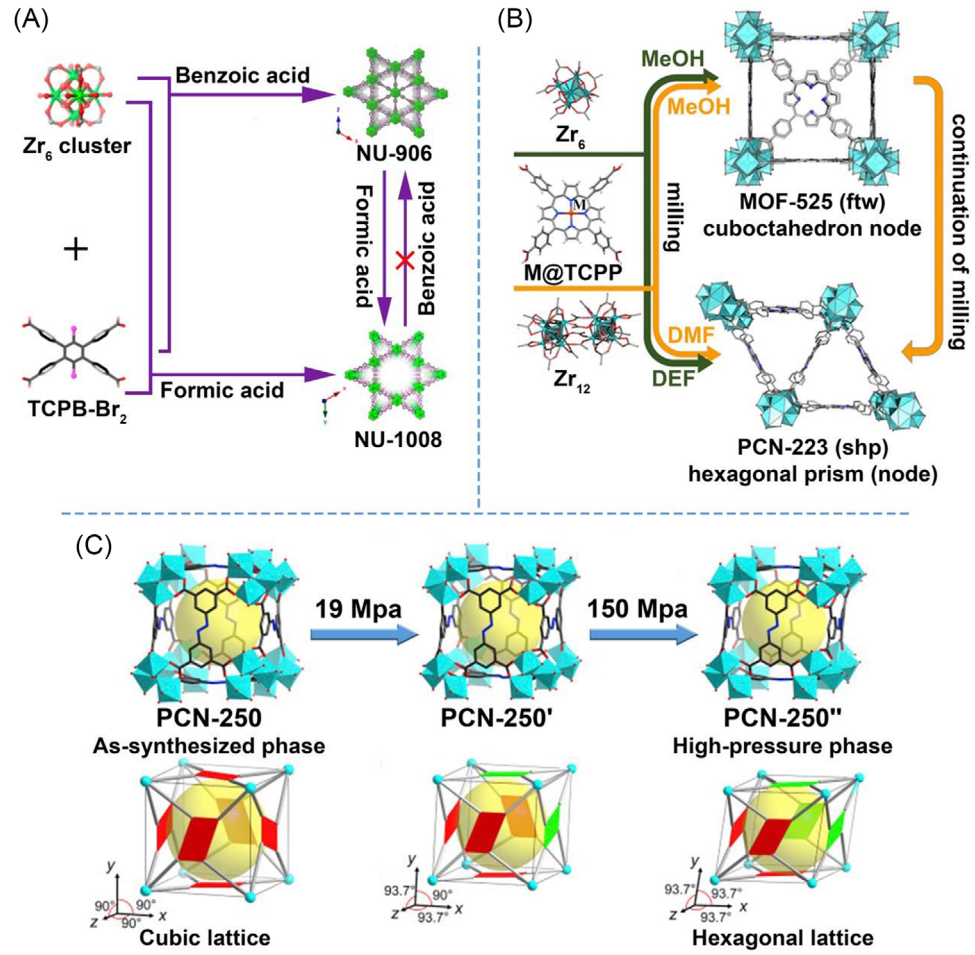

FIGURE 4 Phase transformation of MOFs. (A) The synthesis of NU-1008 and NU-906 from TCPB-Br_2 linker and Zr_6 cluster and the phase transition between NU-1008 and NU-906. Reproduced with permission: Copyright 2019, American Chemical Society.[75] (B) The phase transformation between MOF-525 and PCN-223 by mechanochemical reactions. Reproduced with permission: Copyright 2020, American Chemical Society.[88] (C) Structural transformation of PCN-250 under pressure. Please note that the unit cell of PCN-250′ and PCN-250′′ can be transformed into monoclinic and hexagonal lattices, respectively. However, in this research, they are intentionally indexed into triclinic crystal systems to clearly show the structural transformation under applying pressure. Reproduced with permission: Copyright 2017, Elsevier Inc[40]

3.2 | Phase transformation in MOFs

Phase transformation is an important part of the phase engineering of MOFs and offers an alternative approach to tune the phase of MOFs. Although the research about the phase transformation is essential, it is still at the initial stage. Here, we summarized some representative factors that induce the phase transformation of MOFs, including modulator, solvent, mechanochemistry, and pressure.

3.2.1 | Modulator

In MOFs synthesis, the modulator can not only be used to achieve the phase diversity of MOFs by direct synthesis from the precursors and linkers, but also be employed to induce the phase transformation. For example, the phase transformation from the kinetically stable **hex** EHU-30 to the thermodynamically stable **fcu** UiO-66 has been achieved under the mediation of acetic acid modulator and heating, which was based on a partial dissolution-recrystallization process driven by the realignment of linkers to release strain.[85] Similar phase transformation mechanism was also observed in another work, where irreversible phase transformation from the microporous **scu** NU-906 to the mesoporous **csq** NU-1008 through dissolution-reprecipitation mechanism by soaking NU-906 in a solution of DMF/formic acid under heat treatment (Figure 4A).[75] The formic acid facilitated the dissolution of NU-906 and also acted as a modulator, as a result, the intermediate solution containing Zr_6-clusters, TCPB-Br_2 linkers, formic acid and DMF was formed after the dissolution of NU-906 and led to the generation of NU-1008.

3.2.2 | Solvent

The addition of solvent is also a useful strategy to induce phase transformation of MOFs. For instance, Chen et al. reported that the phase transformation from **fcu** UiO-66 to **hcp** UiO-66 can be achieved by adding a solution of acetic acid and water.[57] Subsequently, by using different acetic acid/water ratio, the authors demonstrated that both acetic acid and water are crucial to this phase transformation. Notably, there was no **hcp** UiO-66 formed when heating the as-synthesized **fcu** UiO-66 in pure DI water even at 150°C, indicating a good stability of **fcu** UiO-66 in pure water. In contrast, if the reaction mixture contains 25 vol% acetic acid and was kept undisturbed under 150°C for 24 h, the **fcu**

UiO-66 would partially transform to **hcp** UiO-66. Such phase transformation from **fcu** UiO-66 to **hcp** UiO-66 could proceed further by simply increasing the acetic acid concentration to 75 vol%. However, if pure acetic acid was used to treat **fcu** UiO-66 at 150°C for 24 h, no **hcp** UiO-66 could be obtained. They proposed that acetic acid could break node-ligands bonds and form node-acetate bonds, whereas water could induce the formation of $Zr_{12}O_{22}$ cluster through the dimerization of the Zr_6O_8 node. In addition, compared with the directly synthesized one, the **hcp** UiO-66 converted from **fcu** UiO-66 showed more defect sites.

3.2.3 | Mechanochemistry

Mechanochemistry, such as ball-milling or grinding, has been successfully applied as an efficient, green, and rapid method to achieve the phase transformation of MOF materials.[86,87] For instance, the liquid-assisted grinding could be used to prepare pure hexagonal **shp** PCN-223 via the phase transformation from cubic **ftw** MOF-525 (Figure 4B).[88] Specifically, when grinding the Zr_{12}-acetate ($Zr_{12}O_8(OH)_8(CH_3COO)_{24}$) cluster with methanol, MOF-525 nuclei formed first and then rapidly transformed to PCN-223. The grinding-induced plastic deformation and the unsaturated coordination provide the MOF-525 nuclei with enough disordering to reconstruct the crystal structure and transform to PCN-223.[88] In addition, as shown in Figure 2A, **hns** UiO-67(Hf) metal-organic nanosheets have also been obtained successfully by grinding or sonication of both **hcp** and **hxl** UiO-67 in methanol, indicating the phase transformation can happen even under mild conditions.[38]

3.2.4 | Pressure

Pressure is also an important parameter to induce the phase transformation of MOFs by distorting the porous structure or the framework of MOFs. The phase of MOFs may transform to an amorphous state under high pressure. For example, Chapman et al. reported that the volume of ZIF-8 framework was compressed quickly by 5% under hydrostatic pressure of 0.34 GPa.[89] With the increase of pressure, the phenomenon of phase transformation from crystalline to amorphous phase was observed. However, Brunauer-Emmett-Teller (BET) test taken at different pressure-treated ZIF-8 samples suggested that the crystallinity of ZIF-8 was progressively eliminated with the increment of pressure from 0.9 GPa to 1.2 GPa. In addition, pressure could also induce the formation of a new high-pressure phase. PCN-250 with a sequential phase transformation under uniaxial mechanical pressure was reported.[40] PCN-250 constructed by Fe_3-μ_3-oxo clusters and 3,3′,5,5′-azobenzenetetracarboxylate (ABTC) possess a **soc** (square–octahedron)[90] net. In PCN-250, each cubic cage is composed of eight corner-sharing Fe-based clusters and six face-sharing ABTC ligands units. As shown in Figure 4C, when uniaxial pressure of 19 MPa was applied, PCN-250 underwent an irreversible phase and 1.26% contraction of framework could be observed. The PCN-250′ (at 19 MPa) with metastable state could transform into a new phase PCN-250′′ when the uniaxial pressure further increased to 150 MPa. Due to the high distortion caused by the flipping of ligands, all lattice angles in PCN-250′′ would no longer be 90° and the unit cell of PCN-250′′ could be converted to hexagonal lattices with higher symmetry.

3.2.5 | Other methods

Besides aforementioned experimental approaches, other methods, like ligand exchange, can also be adopted to induce the phase transformation of MOFs. For example, the phase transformation from **dia-c** (2 fold **dia**[91]) bio-MOF-100 to **lcs**[92] bio-MOF-100 has been investigated by Miera *et al*.[93] The **dia-c**-bio-MOF-100, built from zinc-adeninate ($Zn_8(AD)_4O_{16}$) building units connected by BPDC ligands, was soaked in iridium complexes (IrL) to perform the $BPDC^{2-}$ ligand exchange with IrL^{2-} at room temperature. The phase transformation of bio-MOF-100 from the 2-fold interpenetrated **dia-c** to the non-interpenetrated **lcs** was realized via breaking and re-coordinating of metal-ligand bonds and reassembling the building units within the MOFs. Besides, reversible phase transformation between **hcp** and **hxl** UiO-67(Hf) has been reported (Figure 2A).[38] The phase of as-synthesized UiO-67(Hf) transformed from **hcp** to **hxl** by releasing the $bpdc^{2-}$ ligands under ambient conditions after several days. The obtained **hxl** UiO-67(Hf) is stable under ambient conditions for more than one year. However, if **hxl** UiO-67(Hf) is washed with DMF at 70°C, the **hxl** sheets can be re-connected by the $bpdc^{2-}$ ligands to form **hcp** phase UiO-67(Hf). Similar to **hcp** UiO-67(Hf), the **hcp** UiO-66(Hf) (F_4BDC) can also be converted to a layered **hns** phase by washing the as-synthesized samples with DMF or methanol.[39] Very recently, Zhou et al. reported a phase transformation from CuBDC to Cu_2BDC via a top-down molecular scalpel cleavage strategy.[94] The conventional CuBDC MOFs were chemically cleaved by ascorbic acid to form Cu_2BDC, possessing a different layered structure compared to that of CuBDC. The authors believe ascorbic acid could act as a molecular scalpel to cleave BDC linkers in CuBDC by regulating the chemical state and coordination number of Cu metal centers, leading to the formation of Cu_2BDC.

4 | PHASE-DEPENDENT APPLICATIONS OF MOFS

As a kind of functional porous materials, the potential applications of MOFs have been widely studied. Via affecting the building block arrangement and the local chemical environment of MOFs, phase could alter the physicochemical properties and thus performances of MOFs in different applications. To date, studies of phase-dependent properties of MOFs are still limited. In this section, we summarized recent studies about the applications of MOFs with different phases in the fields of luminescence, absorption and catalysis.

4.1 | Luminescence

The optical applications of MOFs have attracted much research attention in recent years owing to their fascinating

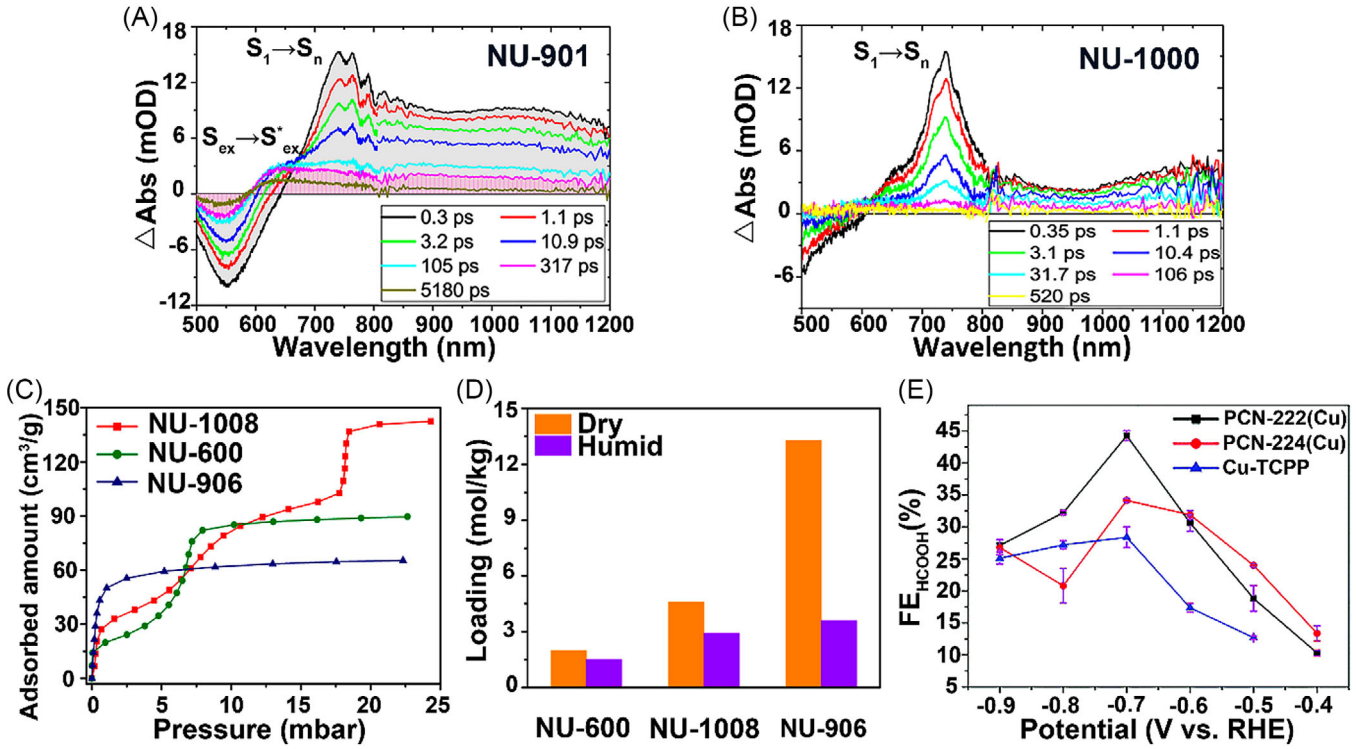

FIGURE 5 Phase-dependent applications of MOFs. (A, B) Femtosecond transient absorption spectra for NU-901 and NU-1000, respectively. Reproduced with permission: Copyright 2018, American Chemical Society.[99] (C) Adsorption isothermal curves of n-hexane for NU-600, NU-906 and NU-1008; (D) 2-Chloroethyl ethyl sulfide loading for NU-600, NU-906 and NU-1008 under dry (0% (relative humidity (RH)) and humid (80% RH) conditions. Reproduced with permission: Copyright 2020, American Chemical Society.[76] (E) The formic acid product faradaic efficiencies of PCN-222(Cu), PCN-224(Cu), and Cu-TCPP for CO_2 reduction. Reproduced with permission: Copyright 2020, The Royal Society of Chemistry[104]

luminescent behaviors.[95,96] The luminescent properties of MOFs could be tuned by the flexible combination of diverse organic/inorganic components, as well as the voids in the MOF.[97] Notably, different phases of MOFs represent various node connectivity and symmetry of the linkers, which could also modify the luminescent performances of MOFs.[58] For example, Deria et al. investigated the phase-dependent emissive properties of two Zr-based MOFs (**scu** NU-902 and **ftw** MOF-525).[98] They found that the emissive spectral properties of MOFs are dependent on the phase of MOFs, which can affect the interchromophoric orientation and interactions and therefore cause the shift of spectra. Specifically, compared to the emission spectra of their free linker in dichloromethane solvent, those of **scu** NU-902 and **ftw** MOF-525 exhibited different extent of red shift. The spectra of **scu** NU-902 showed more red shift than **ftw** MOF-525. The fluorescence lifetime of scu NU-902 (~4.6 ns) was also found to be shorter than that of ftw MOF-525 (~5.6 ns). In another work, Yu et al. reported that MOFs with the same chemical identities but different phases could affect the excited-state electronic structures.[99] Specifically, they found that due to the different inter-linker distance, the **scu** NU-901 and **csq** NU-1000 demonstrated different excited-state properties. As shown in Figure 5A, femtosecond transient absorption (fs-TA) spectroscopy of **scu** NU-901 had an instantaneous $S_1 \rightarrow S_n$ spectral evolution at 750 nm and gradually decreased by the occurrence of the broad induced absorption due to the formation of rapid excimer. However, the fs-TA of **csq** NU-1000 (Figure 5B) showed an obvious difference from that of **scu** NU-901, which only displayed a sharp induced absorption band at 740 nm. Moreover, theoretical calculations predicted that the **csq** NU-1000 had optically allowed charge-transfer states, but this state for NU-901 was forbidden.

4.2 | Adsorption

MOFs are excellent adsorption materials for the removal of pollutants due to their generally high porosity and large surface area.[52,100] Different phases of MOFs could exhibit different porosity and surface area, leading to differences in their adsorption capabilities. For instance, a recent report investigated the abilities of **fcu** UiO-66, defective **fcu** UiO-66 and **hcp** UiO-66 in the removal of perfluorooctanesulfonate (PFOS).[52] The BET test results of the difference MOFs samples showed that defective **fcu** UiO-66 possess a much higher surface area (~1400 m^2/g) than defect-free **fcu** UiO-66 (~1121 m^2/g), while **hcp** UiO-66 exhibited the lowest surface area of ~687 m^2/g, likely due to the cluster condensation in **hcp** UiO-66. The authors found that the PFOS adsorption capacity of MOFs showed a trend of defective **fcu** UiO-66 > **hcp** UiO-66 > defect-free **fcu** UiO 66. Although **hcp** UiO-66 possessed a relatively lower surface area than defect-free **fcu** UiO-66, it exhibited a better PFOS adsorption capacity, which may be attributed to additional small fraction of mesopores (>20 Å) in **hcp** UiO-66. In another report, Garibay et al. studied the capacity of carbon dioxide (CO_2) uptake of NU-901-act (act, HCl activated) and NU-1000-act.[101] It was found that NU-1000-act showed enhanced CO_2 absorption performance compared to NU-901-act, especially at higher absolute CO_2 pressure, indicating that the

pore environment with NU-1000 phase is more accessible for CO_2 uptake.

Difference in pore structures of MOFs with different phases is also an important factor to determine their adsorption abilities. In the work reported by Chen et al., the adsorption abilities of **she**-NU-600, **scu**-NU-906, and **csq**-NU-1008 toward n-hexane and 2-chloroethyl ethyl sulfide (CEES) were studied.[76] The NU-906 has micropores with a diameter of 10.9 Å, which showed steep uptake of n-hexane and could reach saturation at low pressure (Figure 5C). Meanwhile, both NU-600 and NU-1008 have hierarchically porous structures. NU-600 has micropores and mesopores with the diameter of 11.8 Å and 20.0 Å, respectively, while those of NU-1008 are 11.8 Å and 29.5 Å, respectively. Therefore, NU-600 and NU-1008 showed stepwise adsorption behaviors for n-hexane. Particularly, NU-1008 displayed three-step adsorption behavior toward n-hexane, and the adsorption of n-hexane into the larger hexagonal mesopores would cause the narrowing of the mesopores into micropores, leading to a sharp filling at the third step with the highest final uptake of 140.7 cm^3/g. As for CEES adsorption, these MOFs also showed different behaviors under both dry and humid conditions (Figure 5D). Pore size was found to be the key factor in determining the CEES adsorption ability under dry conditions. NU-906 has the smallest pore diameter and showed the highest adsorption ability of CEES with a value of 13.3 mol/kg. NU-1008 has the same 8-connected Zr_6 nodes as NU-906 but a larger pore size and showed a lower CEES loading than NU-906. Under humid conditions, the NU-906 still had the highest CEES uptake ability among these three MOFs. But since the Zr_6 nodes could interact with water and result in a competing uptake of CEES, the NU-906 had a sharp decline of CEES adsorption abilities to 3.6 mol/kg. Compared with NU-906 and NU-1008, NU-600 had the lowest CEES loading under both dry and humid conditions.

4.3 | Catalysis

MOFs are also regarded as a promising group of catalysts for various kinds of catalytic reactions due to their large surface area, well-defined porous structures, versatile structural tunability, and abundant reactive sites.[102,103] Notably, recent studies indicate that the phase of MOFs plays an important role in tuning their catalytic properties. MOFs with different phases and node-connectivity possess alien surface area, pore size and distribution, and density of active sites/defects, which could remarkably affect the mass transformation efficiency, substrate absorption capacity, and utilization of active sites, finally resulting in various catalytic performances.

Chen et al. reported that, compared with **fcu** UiO-66, the **hcp** UiO-66 showed higher catalytic performance towards ring-opening epoxidation reactions with alcohols due to its high densities of defect sites.[57] It was also pointed out that the node-bridging OH groups in **hcp** UiO-66 could be selectively removed during reaction and increased the overall density of active sites, leading to the enhanced catalytic activity. Liu et al. studied the catalytic performance of PCN-222(Cu) and PCN-224(Cu) towards the electrocatalytic CO_2 reduction reaction (CO_2RR) (Figure 5E).[104] Due to the larger specific surface area and pore diameter, PCN-222(Cu) could facilitate more efficient mass transfer during the reaction, leading to improved activity and selectivity for CO_2 reduction to formic acid in the high potential range ($-0.7 \sim -0.9$ V vs. reversible hydrogen electrode (RHE)). However, compared to PCN-222(Cu), PCN-224(Cu) showed a greater heat of adsorption and better affinity for CO_2, promoting the uptake of CO_2 onto the active sites. As a result, PCN-224(Cu) revealed better catalytic activity in the low potential range (-0.4 – -0.6 V vs. RHE). Recently, the photocatalytic CO_2RR performances of three porphyrinic Zr-MOFs with different Zr_6-oxocluster connectivities, including PCN-222, PCN-223, and PCN-224, were investigated by Jin et al.[105] Compared with 8-connected PCN-222 and 12-connected PCN-223, the 6-connected PCN-224 showed the highest formate yield rate, 45.2 μmol g^{-1} h^{-1}. It is worth mentioning that theoretical calculation suggested that PCN-224 had the lowest CO_2 adsorption energy among the three samples, which possibly explained the improved photocatalytic CO_2RR performance of PCN-224.

5 | CONCLUSIONS AND PERSPECTIVES

In summary, we have provided a brief overview of recent advances in phase engineering of MOFs, including direct phase-controlled synthesis and phase transformation of MOFs, as well as the phase-dependent performances of MOFs in luminescence, absorption, and catalysis. To date, direct synthesis is the most common strategy to obtain MOFs with new phases. Among the various kinds of directly synthesized MOFs, Zr- and Hf- based MOFs show the most phase complexity owing to the variable connectivity and symmetry of the Zr- and Hf- based clusters. Compared to the direct synthesis, experimental approaches that can induce phase transformation of MOFs have less been explored, although a few factors such as solvent, pressure, modulator have been reported. With the successful preparations of MOFs with various phases, the role of phase in determining their performances in various applications has also been demonstrated.

Although considerable progress in phase engineering of MOFs has been achieved, there are still some challenges. First, in-depth theoretical insights on the formation and transformation mechanisms of the unconventional phase in MOFs phases are still limited, compared with the relatively extensive experimental studies. Theoretical guidance is highly desired to accelerate the discovery and enable the rational design of MOFs with novel phases. In fact, it has been demonstrated that the computational approach is an efficient way to screen and generate possible MOF structures from given secondary building units and ligands.[106] Second, the synthetic conditions of polymorphic MOFs are usually similar, making it difficult to obtain MOFs with high phase purity in a one-pot synthesis. The lack of methods to prepare MOFs with different phases in high purity is hindering further investigations on the phase-dependent properties of MOFs. Last, investigations on the applications of MOFs with different phases still remain limited. It is believed that more phase-relevant physicochemical properties and applications of MOFs should be studied. In addition, methods to induce the phase transformation of MOFs are still lacking. One key challenge could be the identification of the factors to promote the kinetic control of MOF structures and suppress the thermodynamic control, so that the thermodynamically unfavored

phase of MOFs could be obtained. For example, Maindan et al. found that the different phases of Zr-MOFs constructed by TCPP (Fe^{III}) could affect the redox hopping conductivity of MOF-deposited electrodes.[107] However, the phase-dependent performance of polymorphic Zr-MOFs (Fe^{III}) as photoactive and/or redox-active species in photo- or electrochemical conversions has not been explored.

Despite the abovementioned challenges, there are also opportunities in engineering the phase of MOFs. First of all, apart from the reported methods to obtain MOFs with new phases, other synthetic methodologies should be developed, including but not limited to electrochemical method, photochemical method, microwave radiation-assisted method, magnetic field-assisted method, spray-drying, and flow synthesis. For example, compared with the conventional heating method, microwave radiation-assisted synthesis of MOFs is a more effective and faster heating approach, which can cause the crystallizations at the microwave-induced hot spots.[108] Second, defect engineering could be another effective strategy to obtain MOFs with novel structures. By incorporating ordered defects such as missing linker and/or node into MOFs, novel phases or mixed phases of MOFs may be produced.[109] For example, using the formic acid as a modulator could introduce missing-cluster defects along the < 100 > directions in the **fcu** matrix of UiO-66(Hf), leading to the formation of **reo** UiO-66(Hf) instead of **fcu** UiO-66(Hf).[46] More of such defect-induced phase transformation should be explored. Third, it has been reported that the rational design and synthesis of nanomaterials with heterophase structure will bring enhanced properties in specific applications due to the synergistic effects between different phases, as well as the presence of phase boundaries.[7,110] Hence, developing methods to produce MOFs with well-defined heterophase is another promising research direction. Controllable phase distribution and/or composition of heterophased MOFs, may endow MOFs with intriguing physicochemical properties and broader applications. Fourth, due to the structural complexity and sensitivity of MOFs, advanced analytic technologies are crucial to characterize unconventional phases in MOFs. For instance, the recent development of low electron dose transmission electron microscopy and rotation electron diffraction allows direct and precise structure observation of MOFs.[111,112] Moreover, advancements of in situ observation techniques could further deepen our understanding of the formation and transformation mechanisms of various phases in MOFs. Fifth, the applications of MOFs with unconventional phases can be further explored. Besides luminescence, adsorption, and catalysis, MOFs with unconventional phases may also exhibit enhanced performances in other emerging applications of MOFs, such as biomedicine,[113] mechanical applications,[114] and sensors [115]. Sixth, the concept of PEN can be extended to MOF-based hybrid materials. For example, MOFs with different phases can be used as templates to grow other kinds of organic or inorganic nanomaterials. MOFs with different phases have different pore shape, size, and arrangement, which could be used to control the morphology, size, and even phase of the guest nanomaterials by adjusting the phase of host MOFs. Phase engineering of a rationally designed MOF-based hybrid could further improve their performances toward specific application. Last but not the least, the principles of phase engineering of MOFs can also be used to develop other materials with similar structure complexity such as covalent organic frameworks (COFs) and hydrogen-bonded organic frameworks (HOFs).

ACKNOWLEDGEMENTS

Chen Ma, Long Zheng, Gang Wang, and Jun Guo contributed equally to this work. Y.C. thanks the support from Start-up Fund (Project No. 4930977) and the Direct Grant for Research (Project No. 4053444) from the Chinese University of Hong Kong. H.Z. thanks the support from grants (Project Nos. 9610478, 9680314, 7020013, and 1886921), Start-Up Grant (Project No. 9380100), and ITC via Hong Kong Branch of National Precious Metals Material Engineering Research Center (NPMM) from City University of Hong Kong.

CONFLICT OF INTEREST

The authors declare no conflict of interest.

ORCID

Ye Chen https://orcid.org/0000-0003-0821-7469
Hua Zhang https://orcid.org/0000-0001-9518-740X

REFERENCES

1. Y. Chen, Z. Lai, X. Zhang, Z. Fan, Q. He, C. Tan, H. Zhang, *Nat. Rev. Chem.* **2020**, *4*, 243.
2. S. Lu, J. Liang, H. Long, H. Li, X. Zhou, Z. He, Y. Chen, H. Sun, Z. Fan, H. Zhang, *Acc. Chem. Res.* **2020**, *53*, 2106.
3. H. Li, X. Zhou, W. Zhai, S. Lu, J. Liang, Z. He, H. Long, T. Xiong, H. Sun, Q. He, Z. Fan, H. Zhang, *Adv. Energy Mater.* **2020**, *10*, 2002019.
4. H. Cheng, N. Yang, Q. Lu, Z. Zhang, H. Zhang, *Adv. Mater.* **2018**, *30*, 1707189.
5. Y. Ge, Z. Shi, C. Tan, Y. Chen, H. Cheng, Q. He, H. Zhang, *Chem* **2020**, *6*, 1237.
6. M. Zhao, Y. Xia, *Nat. Rev. Mater.* **2020**, *5*, 440.
7. Z. Fan, M. Bosman, Z. Huang, Y. Chen, C. Ling, L. Wu, Y. A. Akimov, R. Laskowski, B. Chen, P. Ercius, J. Zhang, X. Qi, M. H. Goh, Y. Ge, Z. Zhang, W. Niu, J. Wang, H. Zheng, H. Zhang, *Nat. Commun.* **2020**, *11*, 3293.
8. Y. Chen, Z. Fan, J. Wang, C. Ling, W. Niu, Z. Huang, G. Liu, B. Chen, Z. Lai, X. Liu, B. Li, Y. Zong, L. Gu, J. Wang, X. Wang, H. Zhang, *J. Am. Chem. Soc.* **2020**, *142*, 12760.
9. J. Liu, W. Niu, G. Liu, B. Chen, J. Huang, H. Cheng, D. Hu, J. Wang, Q. Liu, J. Ge, P. Yin, F. Meng, Q. Zhang, L. Gu, Q. Lu, H. Zhang, *J. Am. Chem. Soc.* **2021**, *143*, 4387.
10. Y. Ge, X. Wang, B. Chen, Z. Huang, Z. Shi, B. Huang, J. Liu, G. Wang, Y. Chen, L. Li, S. Lu, Q. Luo, Q. Yun, H. Zhang, *Adv. Mater.* **2022**, *34*, 2107399.
11. M. Zhou, J. Liu, C. Ling, Y. Ge, B. Chen, C. Tan, Z. Fan, J. Huang, J. Chen, Z. Liu, Z. Huang, J. Ge, H. Cheng, Y. Chen, L. Dai, P. Yin, X. Zhang, Q. Yun, J. Wang, H. Zhang, *Adv. Mater.* **2021**, *33*, 2106115.
12. Y. Ge, X. Wang, B. Huang, Z. Huang, B. Chen, C. Ling, J. Liu, G. Liu, J. Zhang, G. Wang, Y. Chen, L. Li, L. Liao, L. Wang, Q. Yun, Z. Lai, S. Lu, Q. Luo, J. Wang, Z. Zheng, H. Zhang, *J. Am. Chem. Soc.* **2021**, *143*, 17292.
13. Y. Yu, G.-H. Nam, Q. He, X.-J. Wu, K. Zhang, Z. Yang, J. Chen, Q. Ma, M. Zhao, Z. Liu, F.-R. Ran, X. Wang, H. Li, X. Huang, B. Li, Q. Xiong, Q. Zhang, Z. Liu, L. Gu, Y. Du, W. Huang, H. Zhang, *Nat. Chem.* **2018**, *10*, 638.
14. L. Liu, J. Wu, L. Wu, M. Ye, X. Liu, Q. Wang, S. Hou, P. Lu, L. Sun, J. Zheng, L. Xing, L. Gu, X. Jiang, L. Xie, L. Jiao, *Nat. Mater.* **2018**, *17*, 1108.
15. Z. Lai, Q. He, T. H. Tran, D. V. M. Repaka, D.-D. Zhou, Y. Sun, S. Xi, Y. Li, A. Chaturvedi, C. Tan, B. Chen, G.-H. Nam, B. Li, C. Ling, W. Zhai, Z. Shi, D. Hu, V. Sharma, Z. Hu, Y. Chen, Z. Zhang, Y. Yu, X. Renshaw Wang, R. V. Ramanujan, Y. Ma, K. Hippalgaonkar, H. Zhang, *Nat. Mater.* **2021**, *20*, 1113.
16. X. Zhang, Z. Luo, P. Yu, Y. Cai, Y. Du, D. Wu, S. Gao, C. Tan, Z. Li, M. Ren, T. Osipowicz, S. Chen, Z. Jiang, J. Li, Y. Huang, J. Yang,

Y. Chen, C. Y. Ang, Y. Zhao, P. Wang, L. Song, X. Wu, Z. Liu, A. Borgna, H. Zhang, *Nat. Catal.* **2018**, *1*, 460.
17. H. Cheng, N. Yang, G. Liu, Y. Ge, J. Huang, Q. Yun, Y. Du, C.-J. Sun, B. Chen, J. Liu, H. Zhang, *Adv. Mater.* **2020**, *32*, 1902964.
18. J. Ge, P. Yin, Y. Chen, H. Cheng, J. Liu, B. Chen, C. Tan, P.-F. Yin, H.-X. Zheng, Q.-Q. Li, S. Chen, W. Xu, X. Wang, G. Wu, R. Sun, X.-H. Shan, X. Hong, H. Zhang, *Adv. Mater.* **2021**, *33*, 2006711.
19. H. Cheng, N. Yang, X. Liu, Q. Yun, M. H. Goh, B. Chen, X. Qi, Q. Lu, X. Chen, W. Liu, L. Gu, H. Zhang, *Natl. Sci. Rev.* **2019**, *6*, 955.
20. N. Yang, H. Cheng, X. Liu, Q. Yun, Y. Chen, B. Li, B. Chen, Z. Zhang, X. Chen, Q. Lu, J. Huang, Y. Huang, Y. Zong, Y. Yang, L. Gu, H. Zhang, *Adv. Mater.* **2018**, *30*, 1803234.
21. O. M. Yaghi, H. Li, *J. Am. Chem. Soc.* **1995**, *117*, 10401.
22. H. Furukawa, K. E. Cordova, M. O'Keeffe, O. M. Yaghi, *Science* **2013**, *341*, 1230444.
23. A. R. Millward, O. M. Yaghi, *J. Am. Chem. Soc.* **2005**, *127*, 17998.
24. J.-R. Li, R. J. Kuppler, H.-C. Zhou, *Chem. Soc. Rev.* **2009**, *38*, 1477.
25. R.-B. Lin, S. Xiang, H. Xing, W. Zhou, B. Chen, *Coord. Chem. Rev.* **2019**, *378*, 87.
26. L. Zhu, X.-Q. Liu, H.-L. Jiang, L.-B. Sun, *Chem. Rev.* **2017**, *117*, 8129.
27. I. Abánades Lázaro, R. S. Forgan, *Coord. Chem. Rev.* **2019**, *380*, 230.
28. X. Jiang, L. Zhang, S. Liu, Y. Zhang, Z. He, W. Li, F. Zhang, Y. Shi, W. Lü, Y. Li, Q. Wen, J. Li, J. Feng, S. Ruan, Y.-J. Zeng, X. Zhu, Y. Lu, H. Zhang, *Adv. Opt. Mater.* **2018**, *6*, 1800561.
29. X.-H. Wu, P. Luo, Z. Wei, Y.-Y. Li, R.-W. Huang, X.-Y. Dong, K. Li, S.-Q. Zang, B. Z. Tang, *Adv. Sci.* **2019**, *6*, 1801304.
30. K. Shen, L. Zhang, X. Chen, L. Liu, D. Zhang, Y. Han, J. Chen, J. Long, R. Luque, Y. Li, B. Chen, *Science* **2018**, *359*, 206.
31. X.-G. Wang, Q. Cheng, Y. Yu, X.-Z. Zhang, *Angew. Chem. Int. Ed.* **2018**, *57*, 7836.
32. M. Zhang, G. Feng, Z. Song, Y.-P. Zhou, H.-Y. Chao, D. Yuan, T. T. Y. Tan, Z. Guo, Z. Hu, B. Z. Tang, B. Liu, D. Zhao, *J. Am. Chem. Soc.* **2014**, *136*, 7241.
33. M. Zhao, Y. Wang, Q. Ma, Y. Huang, X. Zhang, J. Ping, Z. Zhang, Q. Lu, Y. Yu, H. Xu, Y. Zhao, H. Zhang, *Adv. Mater.* **2015**, *27*, 7372.
34. M. Zhao, Y. Huang, Y. Peng, Z. Huang, Q. Ma, H. Zhang, *Chem. Soc. Rev.* **2018**, *47*, 6267.
35. J. Guo, Y. Zhang, Y. Zhu, C. Long, M. Zhao, M. He, X. Zhang, J. Lv, B. Han, Z. Tang, *Angew. Chem. Int. Ed.* **2018**, *57*, 6873.
36. C. Chang, W. Chen, Y. Chen, Y. Chen, Y. Chen, F. Ding, C. Fan, H. J. Fan, Z. Fan, C. Gong, Y. Gong, Q. He, X. Hong, S. Hu, W. Hu, W. Huang, Y. Huang, W. Ji, D. Li, L.-J. Li, Q. Li, L. Lin, C. Ling, M. Liu, N. Liu, Z. Liu, K. P. Loh, J. Ma, F. Miao, H. Peng, et al. *Acta Phys. -Chim. Sin.* **2021**, *37*, 2108017.
37. J. Dong, P. Shen, S. Ying, Z.-J. Li, Y. D. Yuan, Y. Wang, X. Zheng, S. B. Peh, H. Yuan, G. Liu, Y. Cheng, Y. Pan, L. Shi, J. Zhang, D. Yuan, B. Liu, Z. Zhao, B. Z. Tang, D. Zhao, *Chem. Mater.* **2020**, *32*, 6706.
38. M. J. Cliffe, E. Castillo-Martínez, Y. Wu, J. Lee, A. C. Forse, F. C. N. Firth, P. Z. Moghadam, D. Fairen-Jimenez, M. W. Gaultois, J. A. Hill, O. V. Magdysyuk, B. Slater, A. L. Goodwin, C. P. Grey, *J. Am. Chem. Soc.* **2017**, *139*, 5397.
39. F. C. N. Firth, M. J. Cliffe, D. Vulpe, M. Aragones-Anglada, P. Z. Moghadam, D. Fairen-Jimenez, B. Slater, C. P. Grey, *J. Mater. Chem. A* **2019**, *7*, 7459.
40. S. Yuan, X. Sun, J. Pang, C. Lollar, J.-S. Qin, Z. Perry, E. Joseph, X. Wang, Y. Fang, M. Bosch, D. Sun, D. Liu, H.-C. Zhou, *Joule* **2017**, *1*, 806.
41. D. Kim, X. Liu, M. S. Lah, *Inorg. Chem. Front.* **2015**, *2*, 336.
42. M. Li, D. Li, M. O'Keeffe, O. M. Yaghi, *Chem. Rev.* **2014**, *114*, 1343.
43. W. Lu, Z. Wei, Z.-Y. Gu, T.-F. Liu, J. Park, J. Park, J. Tian, M. Zhang, Q. Zhang, T. Gentle Iii, M. Bosch, H.-C. Zhou, *Chem. Soc. Rev.* **2014**, *43*, 5561.
44. Z. Hu, Y. Wang, D. Zhao, *Chem. Soc. Rev.* **2021**, *50*, 4629.
45. J. H. Cavka, S. Jakobsen, U. Olsbye, N. Guillou, C. Lamberti, S. Bordiga, K. P. Lillerud, *J. Am. Chem. Soc.* **2008**, *130*, 13850.
46. M. J. Cliffe, W. Wan, X. Zou, P. A. Chater, A. K. Kleppe, M. G. Tucker, H. Wilhelm, N. P. Funnell, F.-X. Coudert, A. L. Goodwin, *Nat. Commun.* **2014**, *5*, 4176.
47. C. He, K. Lu, D. Liu, W. Lin, *J. Am. Chem. Soc.* **2014**, *136*, 5181.
48. K. Lu, C. He, W. Lin, *J. Am. Chem. Soc.* **2014**, *136*, 16712.
49. R. Xu, Y. Wang, X. Duan, K. Lu, D. Micheroni, A. Hu, W. Lin, *J. Am. Chem. Soc.* **2016**, *138*, 2158.
50. R. Dai, F. Peng, P. Ji, K. Lu, C. Wang, J. Sun, W. Lin, *Inorg. Chem.* **2017**, *56*, 8128.
51. M. Ermer, J. Mehler, M. Kriesten, Y. S. Avadhut, P. S. Schulz, M. Hartmann, *Dalton Trans*. **2018**, *47*, 14426.
52. C. A. Clark, K. N. Heck, C. D. Powell, M. S. Wong, *ACS Sustainable Chem. Eng.* **2019**, *7*, 6619.
53. M. Perfecto-Irigaray, G. Beobide, O. Castillo, I. da Silva, D. García-Lojo, A. Luque, A. Mendia, S. Pérez-Yáñez, *Chem. Commun.* **2019**, *55*, 5954.
54. V. Bon, I. Senkovska, I. A. Baburin, S. Kaskel, *Cryst. Growth Des.* **2013**, *13*, 1231.
55. J. Jacobsen, H. Reinsch, N. Stock, *Inorg. Chem.* **2018**, *57*, 12820.
56. P. Ji, K. Manna, Z. Lin, X. Feng, A. Urban, Y. Song, W. Lin, *J. Am. Chem. Soc.* **2017**, *139*, 7004.
57. X. Chen, Y. Lyu, Z. Wang, X. Qiao, B. C. Gates, D. Yang, *ACS Catal.* **2020**, *10*, 2906.
58. X. Hu, Z. Wang, Y. Su, P. Chen, J. Chen, C. Zhang, C. Wang, *Inorg. Chem.* **2020**, *59*, 4181.
59. K. Li, J. Yang, J. Gu, *Chem. Sci.* **2019**, *10*, 5743.
60. F. Hofmeister, *Archiv f. experiment. Pathol. u. Pharmakol* **1888**, 24, 247.
61. W. Morris, B. Volosskiy, S. Demir, F. Gándara, P. L. McGrier, H. Furukawa, D. Cascio, J. F. Stoddart, O. M. Yaghi, *Inorg. Chem.* **2012**, *51*, 6443.
62. P. Deria, D. A. Gómez-Gualdrón, I. Hod, R. Q. Snurr, J. T. Hupp, O. K. Farha, *J. Am. Chem. Soc.* **2016**, *138*, 14449.
63. D. Feng, H.-L. Jiang, Y.-P. Chen, Z.-Y. Gu, Z. Wei, H.-C. Zhou, *Inorg. Chem.* **2013**, *52*, 12661.
64. D. Feng, Z. Y. Gu, J. R. Li, H. L. Jiang, Z. Wei, H. C. Zhou, *Angew. Chem. Int. Ed.* **2012**, *51*, 10307.
65. D. Feng, Z.-Y. Gu, Y.-P. Chen, J. Park, Z. Wei, Y. Sun, M. Bosch, S. Yuan, H.-C. Zhou, *J. Am. Chem. Soc.* **2014**, *136*, 17714.
66. D. Feng, W.-C. Chung, Z. Wei, Z.-Y. Gu, H.-L. Jiang, Y.-P. Chen, D. J. Darensbourg, H.-C. Zhou, *J. Am. Chem. Soc.* **2013**, *135*, 17105.
67. H.-L. Jiang, D. Feng, K. Wang, Z.-Y. Gu, Z. Wei, Y.-P. Chen, H.-C. Zhou, *J. Am. Chem. Soc.* **2013**, *135*, 13934.
68. F. Nouar, *PhD thesis*, University of South Florida, Los Angeles **2010**.
69. W. Morris PhD thesis, University of California, Los Angeles 2012.
70. X. Gong, H. Noh, N. C. Gianneschi, O. K. Farha, *J. Am. Chem. Soc.* **2019**, *141*, 6146.
71. S. M. Shaikh, P. M. Usov, J. Zhu, M. Cai, J. Alatis, A. J. Morris, *Inorg. Chem.* **2019**, *58*, 5145.
72. Z. Fang, B. Bueken, D. E. De Vos, R. A. Fischer, *Angew. Chem. Int. Ed.* **2015**, *54*, 7234.
73. J. E. Mondloch, W. Bury, D. Fairen-Jimenez, S. Kwon, E. J. DeMarco, M. H. Weston, A. A. Sarjeant, S. T. Nguyen, P. C. Stair, R. Q. Snurr, O. K. Farha, J. T. Hupp, *J. Am. Chem. Soc.* **2013**, *135*, 10294.
74. C.-W. Kung, T. C. Wang, J. E. Mondloch, D. Fairen-Jimenez, D. M. Gardner, W. Bury, J. M. Klingsporn, J. C. Barnes, R. Van Duyne, J. F. Stoddart, M. R. Wasielewski, O. K. Farha, J. T. Hupp, *Chem. Mater.* **2013**, *25*, 5012.
75. J. Lyu, X. Gong, S.-J. Lee, K. Gnanasekaran, X. Zhang, M. C. Wasson, X. Wang, P. Bai, X. Guo, N. C. Gianneschi, *J. Am. Chem. Soc.* **2020**, *142*, 4609.
76. Y. Chen, X. Zhang, M. R. Mian, F. A. Son, K. Zhang, R. Cao, Z. Chen, S.-J. Lee, K. B. Idrees, T. A. Goetjen, *J. Am. Chem. Soc.* **2020**, *142*, 21428.
77. S. Yuan, J.-S. Qin, C. T. Lollar, H.-C. Zhou, *ACS Cent. Sci.* **2018**, *4*, 440.
78. A. Marakulin, A. Lysova, D. Samsonenko, P. Dorovatovskii, V. Lazarenko, D. Dybtsev, V. Fedin, *Russ. Chem. Bull.* **2020**, *69*, 360.
79. V. A. Dubskikh, A. A. Lysova, D. G. Samsonenko, D. N. Dybtsev, V. P. Fedin, *CrystEngComm* **2020**, *22*, 6295.
80. L. Yan, Q. Yue, Q.-X. Jia, G. Lemercier, E.-Q. Gao, *Cryst. Growth Des.* **2009**, *9*, 2984.
81. M. O'Keeffe, M. A. Peskov, S. J. Ramsden, O. M. Yaghi, *Acc. Chem. Res.* **2008**, *41*, 1782.
82. S. Liu, Y. Huang, Q. Dong, H. Wang, J. Duan, *Inorg. Chem.* **2020**, *59*, 9569.
83. Y. Shi, A. J. Cairns, Y. Liu, Y. Belmabkhout, X. Cai, M. Pang, M. Eddaoudi, *CrystEngComm.* **2017**, *19*, 4265.
84. X.-C. Huang, Y.-Y. Lin, J.-P. Zhang, X.-M. Chen, *Angew. Chem. Int. Ed.* **2006**, *45*, 1557.

85. S.-J. Lee, J. L. Mancuso, K. N. Le, C. D. Malliakas, Y.-S. Bae, C. H. Hendon, T. Islamoglu, O. K. Farha, *ACS Mater. Lett.* **2020**, *2*, 499.
86. T. Stolar, K. Užarević, *CrystEngComm.* **2020**, *22*, 4511.
87. A. D. Katsenis, A. Puškarić, V. Štrukil, C. Mottillo, P. A. Julien, K. Užarević, M.-H. Pham, T.-O. Do, S. A. J. Kimber, P. Lazić, O. Magdysyuk, R. E. Dinnebier, I. Halasz, T. Friščić, *Nat. Commun.* **2015**, *6*, 6662.
88. B. Karadeniz, D. Žilić, I. Huskić, L. S. Germann, A. M. Fidelli, S. Muratović, I. Lončarić, M. Etter, R. E. Dinnebier, D. Barišić, N. Cindro, T. Islamoglu, O. K. Farha, T. Friščić, K. Užarević, *J. Am. Chem. Soc.* **2019**, *141*, 19214.
89. K. W. Chapman, G. J. Halder, P. J. Chupas, *J. Am. Chem. Soc.* **2009**, *131*, 17546.
90. Y. Liu, J. F. Eubank, A. J. Cairns, J. Eckert, V. C. Kravtsov, R. Luebke, M. Eddaoudi, *Angew. Chem. Int. Ed.* **2007**, *46*, 3278.
91. E. V. Alexandrov, V. A. Blatov, D. M. Proserpio, *Acta Cryst.* **2012**, *68*, 484.
92. R. Banerjee, A. Phan, B. Wang, C. Knobler, H. Furukawa, M. O'Keeffe, M. Yaghi Omar, *Science* **2008**, *319*, 939.
93. G. González Miera, A. Bermejo Gómez, P. J. Chupas, B. Martín-Matute, K. W. Chapman, A. E. Platero-Prats, *Inorg. Chem.* **2017**, *56*, 4576.
94. X. Zhou, J. Dong, Y. Zhu, L. Liu, Y. Jiao, H. Li, Y. Han, K. Davey, Q. Xu, Y. Zheng, S.-Z. Qiao, *J. Am. Chem. Soc.* **2021**, *143*, 6681.
95. M. D. Allendorf, C. A. Bauer, R. K. Bhakta, R. J. T. Houk, *Chem. Soc. Rev.* **2009**, *38*, 1330.
96. W. P. Lustig, S. Mukherjee, N. D. Rudd, A. V. Desai, J. Li, S. K. Ghosh, *Chem. Soc. Rev.* **2017**, *46*, 3242.
97. J. Dong, D. Zhao, Y. Lu, W.-Y. Sun, *J. Mater. Chem. A* **2019**, *7*, 22744.
98. P. Deria, J. Yu, R. P. Balaraman, J. Mashni, S. N. White, *Chem. Commun.* **2016**, *52*, 13031.
99. J. Yu, J. Park, A. Van Wyk, G. Rumbles, P. Deria, *J. Am. Chem. Soc.* **2018**, *140*, 10488.
100. M.-Y. Gao, B.-Q. Song, D. Sensharma, M. J. Zaworotko, *SmartMat* **2021**, *2*, 38.
101. S. J. Garibay, I. Iordanov, T. Islamoglu, J. B. DeCoste, O. K. Farha, *CrystEngComm* **2018**, *20*, 7066.
102. A. Bavykina, N. Kolobov, I. S. Khan, J. A. Bau, A. Ramirez, J. Gascon, *Chem. Rev.* **2020**, *120*, 8468.
103. S. W. Shuhua Duan, L. Wang, H. She, J. Huang, Q. Wang, *Acta Phys. -Chim. Sin.* **2020**, *36*, 1905086.
104. M. J. Liu, S. M. Cao, B. Q. Feng, B. X. Dong, Y. X. Ding, Q. H. Zheng, Y. L. Teng, Z. W. Li, W. L. Liu, L. G. Feng, *Dalton Trans.* **2020**, *49*, 14995.
105. J. Jin, *New J. Chem.* **2020**, *44*, 15362.
106. C. E. Wilmer, M. Leaf, C. Y. Lee, O. K. Farha, B. G. Hauser, J. T. Hupp, R. Q. Snurr, *Nat. Chem.* **2012**, *4*, 83.
107. K. Maindan, X. Li, J. Yu, P. Deria, *J. Phys. Chem. B* **2019**, *123*, 8814.
108. M. Rubio-Martinez, C. Avci-Camur, A. W. Thornton, I. Imaz, D. Maspoch, M. R. Hill, *Chem. Soc. Rev.* **2017**, *46*, 3453.
109. S. Dissegna, K. Epp, W. R. Heinz, G. Kieslich, R. A. Fischer, *Adv. Mater.* **2018**, *30*, 1704501.
110. Y. Chen, Z. Fan, Z. Luo, X. Liu, Z. Lai, B. Li, Y. Zong, L. Gu, H. Zhang, *Adv. Mater.* **2017**, *29*, 1701331.
111. D. Zhang, Y. Zhu, L. Liu, X. Ying, C.-E. Hsiung, R. Sougrat, K. Li, Y. Han, *Science* **2018**, *359*, 675.
112. S. Leubner, V. E. G. Bengtsson, K. Synnatschke, J. Gosch, A. Koch, H. Reinsch, H. Xu, C. Backes, X. Zou, N. Stock, *J. Am. Chem. Soc.* **2020**, *142*, 15995.
113. R. F. Mendes, F. Figueira, J. P. Leite, L. Gales, F. A. Almeida Paz, *Chem. Soc. Rev.* **2020**, *49*, 9121.
114. N. C. Burtch, J. Heinen, T. D. Bennett, D. Dubbeldam, M. D. Allendorf, *Adv. Mater.* **2018**, *30*, 1704124.
115. H.-Y. Li, S.-N. Zhao, S.-Q. Zang, J. Li, *Chem. Soc. Rev.* **2020**, *49*, 6364.

AUTHOR BIOGRAPHIES

Chen Ma is currently a Ph.D. candidate under the supervision of Assist. Prof. Ye Chen at the Department of Chemistry in The Chinese University of Hong Kong. He obtained his B.Sc. degree from Zhengzhou University and M.S. degree from Technical Institute of Physics and Chemistry, Chinese Academy of Sciences. His research focuses on wet-chemical synthesis of novel low-dimensional nanomaterials.

Ye Chen is currently an assistant professor at the Department of Chemistry, The Chinese University of Hong Kong. She received her B. Eng. and Ph.D. degrees in materials science from Nanyang Technological University (Singapore) in 2015 and 2019, respectively. Her current research interest focuses on wet-chemical synthesis of novel low-dimensional nanomaterials and their applications in catalysis and clean energy.

Hua Zhang received his Ph.D. in Peking University (1998) under the supervision of Prof. Zhongfan Liu. As a Postdoctoral Fellow, he joined Prof. Frans C. De Schryver's group at Katholieke Universiteit Leuven (1999), and Prof. Chad A. Mirkin's group at Northwestern University (2001). After working at NanoInk Inc. and Institute of Bioengineering and Nanotechnology, he joined Nanyang Technological University (2006) and became a full professor (2013). Currently, he is the Herman Hu Chair Professor of Nanomaterials in City University of Hong Kong. His research focuses on the phase engineering of nanomaterials (PEN) and controlled growth of heterostructures for various applications.

How to cite this article: C. Ma, L. Zheng, G. Wang, J. Guo, L. Li, Q. He, Y. Chen, H. Zhang, *Aggregate* **2022**, *3*, e145. https://doi.org/10.1002/agt2.145